Intermolecular Coulomb Decay at Weakly Coupled Heterogeneous Interfaces

Gregory A. Grieves and Thomas M. Orlando

Phys. Rev. Lett. **107**, 016104 — Published 1 July 2011

DOI: 10.1103/PhysRevLett.107.016104

Intermolecular Coulomb decay at weakly coupled heterogeneous interfaces

Gregory A. Grieves[a] and Thomas M. Orlando[a,b,*]

[a] *School of Chemistry and Biochemistry, Georgia Institute of Technology, Atlanta, Georgia USA 30332-0400*

[b] *School of Physics, Georgia Institute of Technology, Atlanta, Georgia USA 30332-0400*

*Corresponding author. Email address: thomas.orlando@chemistry.gatech.edu

Surface ejection of $H^+(H_2O)_{n=1-8}$ from low energy electron irradiated water clusters adsorbed on graphite and graphite with overlayers of Ar, Kr or Xe results from intermolecular Coulomb decay (ICD) at the mixed interface. Inner valence holes in water ($2a_1^{-1}$), Ar ($3s^{-1}$), Kr ($4s^{-1}$) and Xe ($5s^{-1}$) correlate with the cluster appearance thresholds and initiate ICD. Proton transfer occurs during or immediately after ICD and the resultant Coulomb explosion leads to $H^+(H_2O)_{n=1-8}$ desorption with kinetic energies that vary with initiating state, final state and inter-atomic/molecular distances.

PACS numbers: 33.15.-e, 78.47.-p, 68.35.-p, 36.40.Wa, 36.40.-c, 73.20.-r

Electronically excited atoms, molecules and ions are of key importance in plasma physics, radiation physics, astrophysics and planetary atmospheric physics. Therefore, the decay mechanisms of electronic excitations and correlated electron interactions are the subject of intense study, particularly in gas-phase targets.[1, 2] It is well known that electron removal from core levels results in Auger decay and the ejection of electrons. Electron correlation energies and minor Auger electron line-shape changes for core level ionization channels indicate only a slight sensitivity to the environment.[3] More than a decade ago, Cederbaum et al. [2-5] proposed a novel electronic decay mechanism of inner valence levels which should be general in weakly interacting complexes. In the case of complexes involving molecules, this process is referred to as intermolecular Coulomb decay (ICD) and is possible mainly due to the couplings and interactions induced by the local environment. Briefly, ICD follows from the production of an inner valence hole that is filled by an outer valence electron on the same center, followed by energy exchange with a neighbor in the complex and the ejection of an outer valence electron from this neighboring site. Secondary electron emission from the neighboring site can occur as a result of energy transfer via virtual photon exchange. The resulting holes in close proximity then undergo Coulomb repulsion.

A significant amount of the theoretical and experimental work on ICD and correlated energy exchange has concentrated on gas-phase entities such as rare-gas van der Waals dimers.[6-10] Since the ejection of a slow electron is a clear signature of ICD, most of the experimental verifications have focused on the detection of these slow electrons. In a few cases, the separating ion fragments have been detected using co-incidence techniques.[8, 9, 11] Recent work on molecular systems has concentrated on ICD induced ejection of slow electrons during

photoionization of gas-phase water clusters [12] and x-ray photoelectron spectroscopy of aqueous micro-jet solutions.[13]

This Letter reports the first observation of intermolecular Coulomb exchange at a heterogeneous interface between polyatomic contact partners in weakly coupled condensed-phase targets. Specifically, ICD is experimentally demonstrated by examining $H^+(H_2O)_{n=1-8}$ produced via Coulomb explosions during low-energy-electron irradiation of water clusters adsorbed on graphite and 10-20 ML of Ar, Kr or Xe on graphite. For these complicated targets, ICD can involve initial hole formation on different sites (i.e., the rare gas or water cluster) and competitive multielectron decay channels. Depending upon the energetic constraints, ICD is expected to be efficient and general in weakly interacting heterogeneous clusters, condensed-phase surfaces and interfaces.

The experiments were performed in an ultrahigh vacuum (UHV) chamber with a base pressure $\sim 1\times10^{-10}$ Torr, equipped with a pulsed electron gun, time-of-flight spectrometer (TOF) and a quadrupole mass spectrometer (QMS). The electron beam has a typical current density of 10^{14} electrons/cm^{2}s and a beam spot size of ~1.5 mm. The incident electron energy ranged from 5 to 250 eV with an energy spread of ~100 meV. The substrate was mounted in thermal contact with a compressed helium cryostat and heated with a resistive button heater which allowed temperature control from 30 to 500 K. The substrate temperature was maintained and monitored with a thermocouple and a computer-controlled feedback system. The targets were < 1 monolayer (ML) of water deposited on clean HOPG graphite at 30 K or on multilayers of Ar, Kr or Xe pre-adsorbed on graphite. Dosing was carried out with a calibrated pulsed valve using purified degassed water and 99.999% purity rare gases.

Figure 1 shows the $H^+(H_2O)_n$ yields from 0.4 ML of water on 10-20 ML of Ar adsorbed on graphite as a function of incident electron energy (E_i). The back panel displays the cluster ion mass distribution at E_i = 100 eV. The cluster size distribution fits a simple Poisson distribution, suggesting Volmer-Weber island growth on the graphite and rare-gas overlayers. The fit is shown as solid dots in the back panel in figure 1. The protonated clusters desorbing from islands probably do not encounter the dielectric screening and escape barriers typical of ice.[14] Therefore the observed cluster sizes reflect the nascent distribution which depends upon the total coverage. For > 10 ML rare-gas substrates, the peak water cluster ion signal occurs for water coverages < 0.5 ML.[15, 16] At higher water coverage, the cross section for cluster-ion production and desorption drops, with removal of the small clusters being the least probable. Most of the data presented have been taken at water coverages < 0.5 ML.

Several important observations should be pointed out: i) the cluster distribution is the same for water adsorbed on graphite and on all the rare gas substrates, ii) the cluster ion yield is more than an order of magnitude greater for water clusters adsorbed on the rare gases vs. graphite, iii) the $H^+(H_2O)_n$ distribution observed at 100 eV does not change as a function of incident electron energy (i.e. it is the same even in the threshold region) and iv) each cluster has the same threshold energy.

The left panel of figure 1 shows an example of the threshold data for $H^+(H_2O)_{n=4}$ (the most intense cluster peak) formation and desorption from a $(H_2O)_n$:Ar/graphite substrate. The threshold energies for direct ejection of $H^+(H_2O)_{n=4}$ from all the targets are shown in the left side panels of figure 2. The data are represented by solid symbols while results from an established threshold fitting procedure are shown with lines.[17] The fitting function is given by $I(E) = I_0 \frac{(E - E_0)^p}{E^{1/2}}$ where I(E) is the threshold intensity function, E_0 is the threshold energy and

$1 < p \leq 2$ is a free parameter. The fit works well for graphite and Ar, but reduces in quality with increasing rare gas size. Thus, for the case of Kr and Xe, accurate fitting required the sum of two of these functions. The fitting procedure (see insets) yields primary threshold energies of 35 ± 2 eV, 29 ± 2 eV, 29.8 ± 2 eV and 23 ± 2 eV for $H^+(H_2O)_n$ from < 0.5 ML of $(H_2O)_n$ on graphite and Ar, Kr and Xe covered graphite, respectively. The closest single-hole state in water is the $2a_1^{-1}$ centered at ~ 32 eV.[12] Since surface states of condensed rare-gases maintain significant gas-phase character, the 29, 29.8 and 23 eV threshold energies likely correlate with the slightly perturbed Ar $3s^{-1}$ (29.3 eV), Kr $4s^{-1}$ (27.5 eV) and Xe $5s^{-1}$ (23.3 eV) excitations, respectively.

The frames on the right of figure 2 show representative $H^+(H_2O)_4$ kinetic energy (KE) distributions. For water clusters on pure graphite, the KE peaks at ~ 5 eV and extends to ~ 11 eV. For the $(H_2O)_n$:Ar/graphite substrate, the $H^+(H_2O)_4$ KE peak shifts to 1.7 eV and has a defined shoulder at 1.6 eV. A similar two-component distribution is observed for the $(H_2O)_n$:Kr/graphite substrate with a primary peak at 1.5 eV and secondary at 1.4 eV. The $(H_2O)_n$:Xe/graphite substrate yields a single component distribution with a peak near 1.55 eV. The low threshold energies and slow KE distributions (relative to multilayer water) indicate that formation and desorption of $H^+(H_2O)_n$ from <0.5 ML of $(H_2O)_n$ on graphite and Ar, Kr and Xe covered graphite substrates involves ICD. Though the observed cluster sizes reflects the nascent deposited cluster distribution, the two-component energy distributions reflect the initial hole identities and eventual charge locations produced via ICD.

The threshold behavior of an ICD process can be strongly affected by the overlapping density of states in the initial inner valence hole and the two-center two-hole final state.[3] The rare gas inner valence ns^{-1} holes decay producing holes in the corresponding Ar, Kr and Xe *np* levels. During this process ~15, 13 and 11 eV can be transferred, respectively, to adjacent water

clusters via ICD. Note that 15 and 13 eV can ionize both the $1b_1$ and $3a_1$ levels of water. However 11 eV available from decay of the Xe $5s^{-1}$ is barely enough for ionization of the $1b_1$ level in small water clusters, and is close to the minimum energy for creating a $1b_1$ hole in larger water clusters (i.e. $(H_2O)_{n\geq 7}$). [18] Since all the observed clusters are protonated, proton transfer must occur either during the ICD event or immediately afterwards. This is consistent with molecular dynamics simulations that indicate proton transfer in < 50 fs following ionization.[19, 20] The protonated water cluster ions are then ejected by Coulomb repulsion primarily with the hole in the p-orbital of the rare gas.

The primary thresholds using Ar, Kr and Xe substrates are fit reasonably well at the rare gas ns^{-1} threshold energies indicating a narrow spread between the initial state and the two-site final states governed by the overlap given by $\left\langle 1b_1^{-1}, np^{-1} \middle| H \middle| ns^{-1}, X \right\rangle$ (eq. 1a) and $\left\langle 3a_1^{-1}, np^{-1} \middle| H \middle| ns^{-1}, X \right\rangle$ (eq. 1b), where X is the ground electronic state of H_2O and the wavefunctions are denoted as $\left| RG, H_2O \right\rangle$, and H is the interaction Hamiltonian as described in [3]. This is illustrated schematically in figure 3 by arrows labeled 1a and 1b. Note that though there is some signal near 24 eV for Kr, this is a very weak appearance threshold that can be associated with the minimum energy for a two-hole state located on separate water molecules. This can be produced by ICD involving pure water clusters but this has a very low cross section.[12] The primary 29.8 ±2 eV threshold is close to the unperturbed Kr $4s^{-1}$ level. The threshold behavior for the $(H_2O)_n$:Xe/graphite substrate is similar with a low energy threshold near ~ 23 eV followed by a steeper secondary rise at ~ 28 eV. The low energy threshold may also correspond to the minimum two-hole two-site energy for pure water but given the intensity and slope shown in the inset, it more likely corresponds to ICD involving the Xe $5s^{-1}$ level. The increase near 28 eV can be explained if ionization of the $2a_1$ level of water becomes accessible.

These additional decay channels are given by $\left\langle 1b_1^{-1}, np^{-1} \middle| H \middle| ns, 2a_1^{-1} \right\rangle$ (eq. 2a), and $\left\langle 3a_1^{-1}, np^{-1} \middle| H \middle| ns, 2a_1^{-1} \right\rangle$ (eq. 2b), and are also denoted in figure 3. These channels may be operative in the Ar and Kr systems but are embedded in an already strong continuum signal and are not as clear as in the Xe system. Although the case of a heterogeneous interface is complicated by the availability of multiple decay channels and several possible final states, the overall process should still occur at most weakly coupled heterogeneous targets, provided there is energy and density overlap of the two-hole, two-site final state and the single hole initial state.

Hole energetics and their relative spatial proximities can be revealed by the observed KE distributions shown in figure 2. The KE distribution from $(H_2O)_n$ on pure graphite is essentially the same as that observed from pure multilayer water ice. In the latter case, $H^+(H_2O)_n$ was attributed to a Coloumb explosion from an initial $2a_1^{-2}$ state that decayed into configurationally mixed single hole states on two neighboring water sites.[14] A similar two-hole, two-site final state can also be produced by ICD from an initial hole in the $2a_1$ level. As noted above, for Ar and Kr substrates, sufficient energy is available during ICD to access either a $1b_1^{-1}$ or $3a_1^{-1}$ hole on the water. This can lead to broad KE distributions with fast and slow components. Decay of the $5s^{-1}$ state in the $(H_2O)_n$:Xe/graphite system yields just enough energy to create a $1b_1^{-1}$ hole on the $(H_2O)_n$ leading to a single narrower KE distribution. The less intense slow component for Ar and Kr substrates can be explained by a shorter $3a_1^{-1}$ hole lifetime, which is expected due to the increased hole hopping associated with bands of a_1 symmetry in ice and the extended distance where Coulomb repulsion occurs relative to the point of origin. The more intense fast component is more likely correlated with the $1b_1^{-1}$ state. [14]

The general distance dependence of ICD falls as $\sim 1/R^6$ which strongly selects for the first coordination shell.[3] Outside this, it likely drops off more rapidly due to solvation effects.

The density of states near the final state of the ICD resonance dominates the decay cross section within the first shell. This would typically result in the highest kinetic energy from the smallest rare gas substrate and the highest yields from the largest rare gas partner due to closer level spacing and higher density of states in the threshold region. This is consistent with our observations. In addition, since the final two-hole, two-site configuration just prior to Coulomb explosion is probably a protonated water cluster separated from the rare gas ion by an OH fragment, the resulting kinetic energies can be shifted to lower values by the additional separation associated with this neutral fragment.

ICD results in the localized formation of energetic reactive ionic fragments and low energy secondary electrons and thus can contribute to radiation damage of biological targets. [12, 21-26] The ionic fragments can induce DNA damage via ion-molecule reactions and the < 5 eV electrons induce single-strand breaks (SSBs) in DNA via shape resonances.[26] Since ICD can produce at least two reactive fragments and a > 20% yield of < 5 eV electrons, ICD may contribute up to ~ 50% of the SSB probability for > 20 eV ionization events directly at the DNA:water interface.[12] Note the formation of double strand breaks (DSBs) requires excitation energies > 5 eV, thus the impact on the DSB probability is expected to be lower. [21, 26]

In summary, we report the observation of ICD at a heterogeneous interface between polyatomic collision partners in weakly coupled condensed-phase targets. Specifically, ICD is experimentally demonstrated by examining $H^+(H_2O)_{n=1-8}$ produced via Coulomb explosions during low-energy electron-irradiation of water clusters adsorbed on graphite and 10-20 ML of Ar, Kr or Xe on graphite. Inner valence holes in water ($2a_1$), Ar (*3s*), Kr (*4s*) and Xe (*5s*) levels initiate ICD. Proton transfer occurs during or immediately after ICD and the resultant Coulomb

explosion leads to $H^+(H_2O)_{n=1-8}$ with kinetic energies that vary with initial and final inter-ion distance.

The authors gratefully acknowledge support from the US Department of Energy, grant No. DE-FG02-02ER15337.

References

[1] G. Ohrwall *et al.*, Phys. Rev. Lett. **93**, 173401/1 (2004).
[2] L. S. Cederbaum, J. Zobeley, and F. Tarantelli, Phys. Rev. Lett. **79**, 4778 (1997).
[3] R. Santra, J. Zobeley, and L. S. Cederbaum, Phys. Rev. B **64**, 245104/1 (2001).
[4] J. Zobeley, L. S. Cederbaum, and F. Tarantelli, J. Phys. Chem. A **103**, 11145 (1999).
[5] R. Santra *et al.*, Phys. Rev. Lett. **85**, 4490 (2000).
[6] S. Scheit *et al.*, J. Chem. Phys. **121**, 8393 (2004).
[7] K. Kreidi *et al.*, J. Phys. B At., Mol. Opt. Phys. **41**, 101002/1 (2008).
[8] P. Lablanquie *et al.*, J. Chem. Phys. **127**, 154323/1 (2007).
[9] T. Jahnke *et al.*, Phys. Rev. Lett. **93**, 163401/1 (2004).
[10] Y. Morishita *et al.*, Phys. Rev. Lett. **96**, 243402/1 (2006).
[11] T. Jahnke *et al.*, Nature Physics **6**, 139 (2010).
[12] M. Mucke *et al.*, Nature Physics **6**, 143 (2010).
[13] C. P. Schwartz *et al.*, Phys. Rev. Lett. **105**, 198102 (2010).
[14] J. Herring-Captain *et al.*, Phys. Rev. B **72**, 035431/1 (2005).
[15] T. Tachibana, T. Miura, and I. Arakawa, Low Temp. Phys. **32**, 1092 (2006).
[16] R. Souda, Surf. Sci. **506**, L275 (2002).
[17] W. B. Maier, II, J. Chem. Phys. **41**, 2174 (1964).
[18] J. Coe *et al.*, J. Chem. Phys. **107**, 6023 (1997).
[19] H. Tachikawa, J. Phys. Chem. A **108**, 7853 (2004).
[20] A. Furuhama, M. Dupuis, and K. Hirao, J. Chem. Phys. **124**, 164310/1 (2006).
[21] Y. Chen, A. Aleksandrov, and T. M. Orlando, Int. J. Mass Spectrom. **277**, 314 (2008).
[22] L. Caron *et al.*, Phys. Rev. A At., Mol., Opt. Phys. **80**, 012705/1 (2009).
[23] X. Pan *et al.*, Phys. Rev. Lett. **90**, 208102/1 (2003).
[24] T. M. Orlando *et al.*, J. Chem. Phys. **128**, 195102 (2008).
[25] Z. Deng *et al.*, Phys. Rev. Lett. **96**, 243203 (2006).
[26] F. Martin *et al.*, Phys. Rev. Lett. **93**, 68101 (2004).

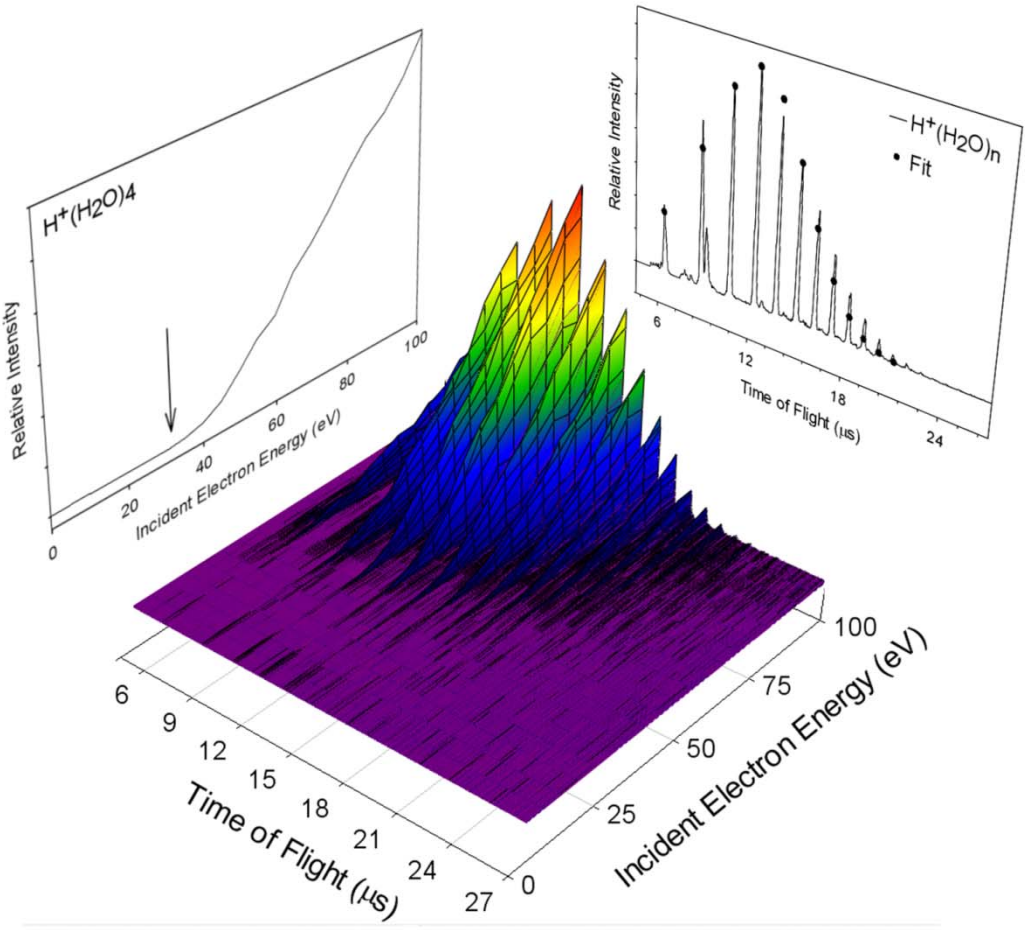

Figure 1. (Color online) The flight time distribution of protonated water clusters measured from 0.4 ML water adsorbed on multilayers of argon as a function of incident electron energy (E_i). Back panel right shows the projection of the mass spectrum taken at E_i = 100 eV. The dots show a fit to a Poisson distribution suggesting that clusters are sampled from the nascent distribution on the surface. Back panel left shows the projection of the $H^+(H_2O)_4$ cluster from the distribution versus energy and shows the onset threshold.

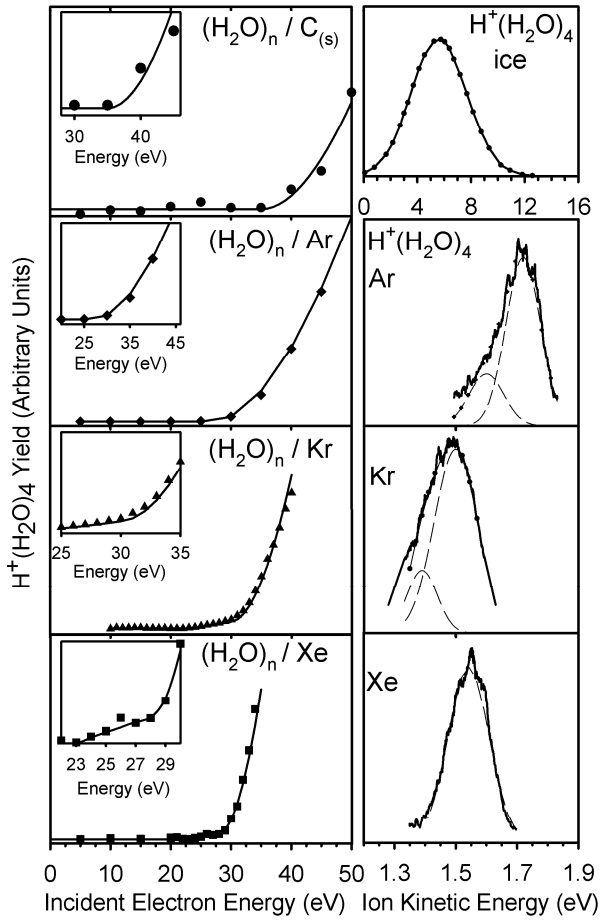

Figure 2. (Left panel) $H^+(H_2O)_n$ threshold data for submonolayer films of water on graphite, Ar, Kr and Xe. Insets show magnified view of threshold region with data as solid points and threshold fit as solid lines. (Right panel) Cluster kinetic energy for the selected cluster $H^+(H_2O)_{n=4}$. Dotted and dashed lines are fits to the kinetic energy

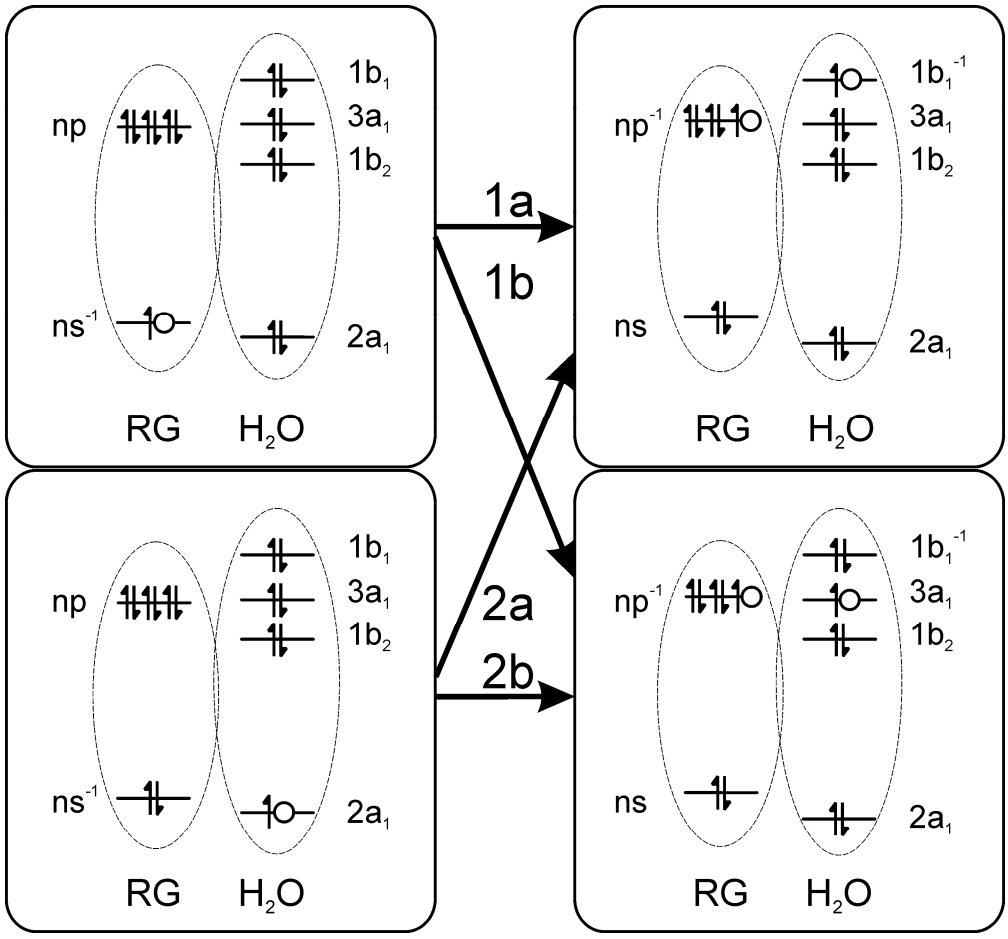

Figure 3. State correlation diagram for ICD induced formation of protonated water clusters adsorbed on a condensed rare gas surface. Incident electrons create initial inner valence holes (left). The inner valence hole states either on the rare gas *s* or water $2a_1$ level can decay as an outer valence electron on the same site falls in to fill it. The resulting energy released by this process can couple to a contacting neighbor causing it to ionize one of its outer valence electrons (right).